JET PROPULSION LABORATORY **INTEROFFICE MEMORANDUM**

ADF-590-REVISED

TO: AIRS Design File **DATE:** 27 September 2002

FROM: Mark Hofstadter

SUBJECT: First Vis/NIR Vicarious Gain Calibration

KEYWORDS: Vis/NIR, Calibration, Validation, Railroad Valley

ABSTRACT: The first accurate determination of instrument gains for the Vis/NIR detectors has been completed via "vicarious calibration". This report details the procedures and results of that effort. We find detector-to-detector gain variations within a channel are typically less than 1%, and average gains are 0.5470, 0.2208, 0.1723, and 0.1922 (±10%) W m^{-2} $micron^{-1}$ $ster^{-1}$ per instrument count, for channels 1 to 4, respectively. **The original ADF-590, dated 13 September, has been updated to correct an error in Tables IV and V.**

1. Introduction

Due to funding and schedule constraints, the Vis/NIR detectors were not radiometrically calibrated prior to launch. This was acceptable because the primary Vis products (cloud and surface variability flags) could be generated without accurate knowledge of instrument gains. It was recognized, however, that absolute calibration could be performed after launch using observations of well characterized ground sites, and that such information would improve the products. A "vicarious calibration" effort was therefore written into the on-orbit checkout plans. In June and July of 2002, we coordinated with an existing MISR-Terra field experiment in Railroad Valley Playa to carry out our first calibration. The results are presented below. We expect this effort to be repeated periodically (once or twice a year) to validate the existing calibration and to track changes in instrument performance.

2. Field Data

The MISR-Terra calibration team, working closely with MODIS-Terra, has identified a region of Railroad Valley Playa in Nevada as a good target for vicarious calibrations. The center of the field area is located at 38˚ 30.30′ N latitude (38.505˚ N), and 115˚ 41.34′ W longitude (115.689˚ W). A team was at the site for much of June and July 2002, supporting both Aqua and Terra spacecraft overflights. There were two Aqua overpasses suitable for vicarious calibration (having the right combination of viewing geometry, clear skies, and working instruments both on the ground and in orbit), on June 10 and 11th 2002. The MISR team collected field data, calibrated it, and converted it to physical properties as described at their web-site,
http://www-misr.jpl.nasa.gov/mission/valwork/mivalres.html#techdata.

The MISR team also ran their forward model to provide calculated top-of-atmosphere (TOA) radiances for the exact AIRS viewing geometry, using the Vis/NIR spectral response functions as reported in ADF-479. Their report is attached as an appendix. Their forward model has been validated against the forward model used by MODIS, with

near-perfect agreement. A "sanity check" comparison between the MISR model and UCSB's SBMOD was also made, again with good results. (The UCSB model was run with slightly different aerosol and water vapor conditions due to limitations on the input parameters accepted by SBMOD, and possibly with a different solar model. SBMOD has previously been tested against the MODIS model with agreement to within a few percent.) The MISR calculated TOA radiances, summarized in Table I, are believed to be good to 5%, neglecting possible errors in the Vis/NIR spectral response function. Radiance differences between the two days are due to the different solar/spacecraft geometries and differences in atmospheric water and aerosol loading.

Table I: Summary of Observing Geometry and Model Radiances

Date in June	Time (UTC)	Solar Zenith (deg)	Solar Azimuth* (deg)	S/C Zenith (deg)	S/C Azimuth* (deg)	TOA Radiance (W m^{-2} $ster^{-1}$ $micron^{-1}$)			
						Ch. 1	Ch. 2	Ch. 3	Ch. 4
10	20:19	17.68	212.33	45.57	75.3	129.2613	155.7759	116.6813	129.2011
11	20:56	23.06	234.08	21.58	260.87	144.6209	181.9092	133.8255	149.1061

*Azimuth measured Eastward (CW) from due North

While the spacecraft zenith angle was much better on June 11th, the spacecraft was also near the direct backscatter peak from the sun, called the hot-spot. The surface reflectance in the hot-spot region is not well characterized because the PARABOLA instrument (used to measure BRDF) casts its shadow in that direction. Also, while both days were quite clear and dry, the 10th was even more so than the 11th. For these reasons, the data of June 10th are considered more reliable by the MISR team.

3. Spacecraft Data

Figure 1 is a map-projected image of Railroad Valley Playa. It is approximately 15 km across, and high resolution aircraft images (Air-MISR) show it to have reflectivity variations of ~10% across it. The field-site chosen is in a relatively homogeneous part of the playa, approximately 2 km across, making it a (barely) acceptable target for the 2.3 km Vis/NIR footprint.

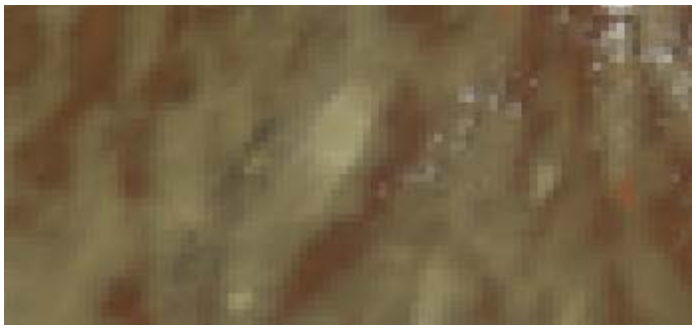

Figure 1: Vis/NIR image of Railroad Valley Playa. The playa is the bright oval region in the center of the image, approximately 10 pixels across. The mapping algorithm smoothes the data, so the pixels seen here are different than the instantaneous footprints of the instrument. (The projection is shown to facilitate comparisons with other data sets.) The field site is in the slightly darker region to the left of the playa center. The image is a color composite of offset-subtracted counts from Vis/NIR channels 1, 2, and 3 as blue, green, and red, respectively. Channel 3 is particularly sensitive to wavelengths reflected by plants, causing the more vegetated hills to appear brown/red in this image. White spots in the upper right are clouds. This image is from 15 June 2002, Granule 205. Images made on June 10th and 11th are similar.

Because the field-site fits within one Vis/NIR pixel, and because the surrounding region is known to have a different reflectivity, we are most interested in the pixel whose center is closest to the center of the field site. Table II presents this information for Granule 203 of June 10th and Granule 210 of June 11th, the optimal overpasses of this campaign. In the table, the location shown for June 10th is from Channel 3, while that of June 11th is for Channel 1. The geolocation of each channel is slightly different, particularly for off-nadir viewing, but the line and sample number closest to the field site is the same for all channels. (Line and sample are one-based numbers giving the location of the pixel in instrument coordinates within the granule. Line 1, Sample 1 is the south-west [lower-left] corner of the granule.) For future reference, it should also be noted that each channel has 9 detectors aligned along-track which are scanned across the swath. Thus, all samples of a given line come from one detector. Line 1052 (June 10th) corresponds to one-based Detector 8, and line 717 (June 11th) corresponds to Detector 6, where detectors are numbered with 9 being furthest along-track (north).

Table II: Observed Instrument Counts

Date	Lat (˚ N)	Lon (˚ W)	Line	Sample	Instrument Counts (offset term removed)*			
					Ch 1	Ch 2	Ch 3	Ch 4
June 10	38.498436	115.68146	1052	65	235.635	701.143	676.187	674.913
June 11	38.496758	115.69576	717	499	280.722	840.235	797.143	799.353

*Instrument counts (offset subtracted) are from L1b product files, PGE version v2.3.3.2

4. Initial Gain Determination

To determine instrument gains, one merely divides the calculated TOA radiance from Table I by the observed counts from Table II. This calibrates one of the 9 detectors in each channel. (Extrapolating results to other detectors is discussed in the next section.) The resulting gains are shown in Table III. We note that the data from the two days agree to within 3% of each other for all channels except Channel 1, where the difference is 6%. This is reasonable given the 5% error-bars estimated by the MISR team. Since the data from June 10th are considered more reliable (see Section 2), we will use that day's results rather than an average of the two days.

Table III: Single-Detector Gain Estimates

Date	Detector (one-based)	Gain (W m^{-2} $ster^{-1}$ $micron^{-1}$ per count)			
		Channel 1	Channel 2	Channel 3	Channel 4
June 10	8	0.5486	0.2222	0.1726	0.1914
June 11	6	0.5152	0.2165	0.1679	0.1865

5. Relative Gain Determination

In the previous section we calibrated one of the nine detectors in each channel. To determine gains for the other 8 detectors in each channel, we need to know their relative gains. We determined this by using scene data. Over a large, homogeneous surface, one would expect the average TOA radiance to be the same in each of the 9 detectors of a channel, as long as systematic viewing geometry effects are small (for example, the spacecraft zenith angle is approximately 0.8˚ larger for detectors 1 and 9 than it is for detector 5). Detector-to-detector differences in average counts (offset subtracted) are then a measure of relative gain variations. We therefore selected several regions for

study and averaged the observed counts (offset subtracted) for each detector of each channel. Regions selected were in both the Northern and Southern Hemisphere (to look for systematic effects caused by solar zenith angle), near nadir, and over both homogeneous ocean and bright desert surfaces. Figure 2 shows what we consider to be the best region for study. It is in the Sahara Desert, near the Egyptian-Libyan border, and appears extremely uniform. Our best Southern Hemisphere region is in the Kalahari Desert (Fig. 3) which, while less uniform, covers a much larger area allowing averaging to smooth out surface inhomogeneities. Other regions tested include the Red Sea, Gulf of Carpentaria (along Australia's north coast), and small, bright desert patches in South Africa. These other regions yielded "noisier" relative gains (due to lower signal levels or higher standard deviations within the sample), so we ignore them given the outstanding agreement between the Sahara and Kalahari samples.

The relative signal-level (which is the inverse of the relative gain) for each detector is shown in Table IV for the two sample regions of Figs 2 and 3. Note the excellent agreement between the two days (to within 0.3%) for all channels except Channel 1, where the agreement is to within 1.3%. Since the signal level in Channel 1 is lowest, and this channel is most sensitive to aerosols, it is not surprising that it is the most uncertain. The consistency of these results gives us confidence that the detector-to-detector variations of ~1% within channels 2 to 4 are real. Since visual inspection of the images, as well as the standard deviation of counts within each sample indicate the Sahara test region is most uniform, we will adopt its values for the relative signal levels.

Table IV: Signal Level Relative to Detector 8

Detector	Signal Relative to (one-based) Detector 8							
	Channel 1		Channel 2		Channel 3		Channel 4	
	Sahara	Kalahari	Sahara	Kalahari	Sahara	Kalahari	Sahara	Kalahari
1	1.003	1.016	1.014	1.014	1.002	1.003	0.993	0.994
2	1.004	1.013	1.012	1.012	1.001	1.003	0.993	0.993
3	1.005	1.012	1.011	1.010	1.005	1.005	0.994	0.993
4	1.005	1.011	1.010	1.012	1.006	1.009	0.994	0.996
5	1.005	1.009	1.008	1.009	1.004	1.006	0.996	0.997
6	1.005	1.009	1.005	1.007	1.002	1.003	0.998	0.999
7	1.002	1.004	1.002	1.003	1.001	1.001	1.000	1.001
8	1.0	1.0	1.0	1.0	1.0	1.0	1.0	1.0
9	0.997	0.996	0.997	0.998	0.994	0.996	0.998	0.999

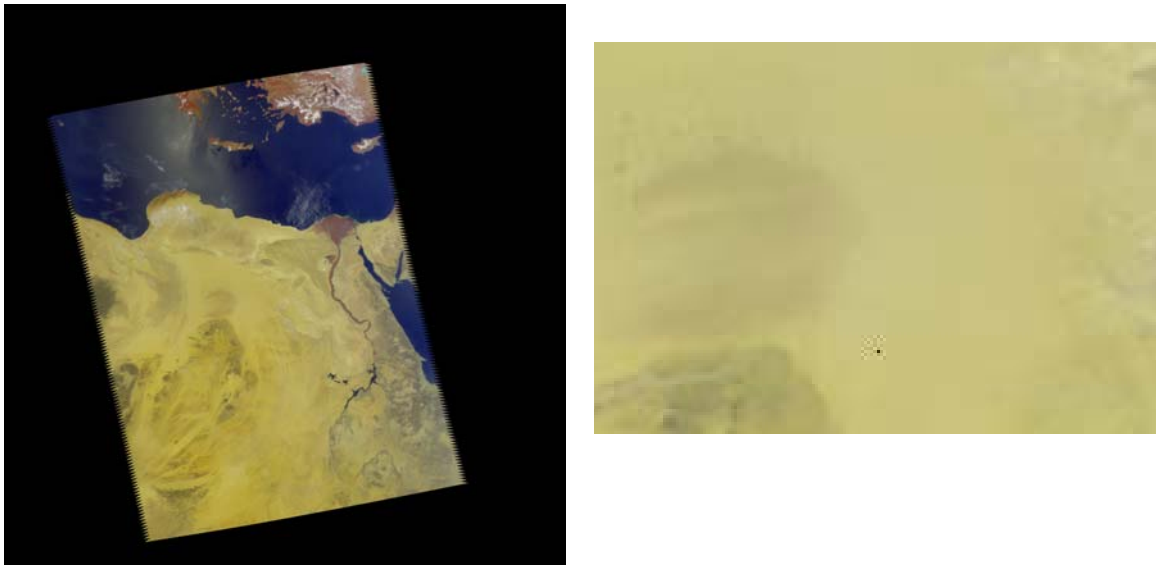

Figure 2: Sample region in the Sahara Desert. On the left is the entire Granule 115 of 14 June 2002. Near the center of the granule is a bright desert patch, west of the Nile and just east of a dark patch due south of Crete. A detail of the region is shown on the right: samples come from the region to the south-east of the dark patch on the middle-left edge of the frame. Both images are color composites using Vis/NIR channels 1, 2, and 3 as blue, green, red, respectively. The exact region used is square in instrument coordinates, encompassing across-track IR footprints 39 to 45, and along-track scanlines 64 to 67. This provides a sample of 224 Vis pixels for each of the 9 detectors in each channel. While not square in map coordinates, the lower left corner of the region is at 26.547˚ N, 25.693˚E, and the upper right corner is at 27.452˚N, 26.521˚E.

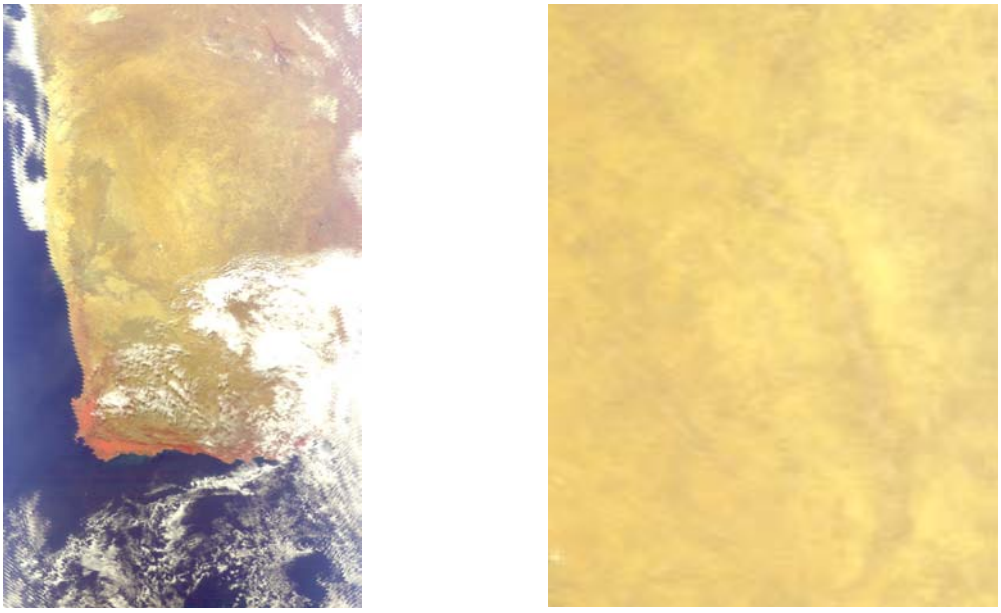

Figure 3: Sample region in the Kalahari Desert. On the left is the entire Granule 124 of 20 July 2002. It is displayed in instrument coordinates, so sampling affects appear off-nadir. The region chosen is the mottled but relatively bright region above center on the left, and is shown in detail on the right. It consists of IR footprints 38 to 49, and scanlines 83 to 97, providing 1440 Vis pixels for each of the 9 detectors in each channel.

6. Final Gain Determination and Error Bars

By combining the June 10th gain determination for Detector 8 (Table III), and the relative signal levels of the "Sahara" column of Table IV, we can determine our final gain estimate for all detectors and channels of the Vis/NIR system. The results are presented in Table V. (Remember that the values in Table IV represent the inverse of the relative gains of each detector.) Based on the discussions above, we believe one-sigma relative error bars within each channel are 1% in Channel 1, and 0.3% in Channels 2-4. Absolute errors are 10% and 5%, respectively. This neglects possible errors in the spectral response functions assumed for these calculations. From ADF-479, such errors could place an additional bias of up to ~5% on each channel, making the total absolute errors 11% and 7%, respectively.

Table V: Final Gain Determination

Detector	Gain (W m^{-2} $ster^{-1}$ $micron^{-1}$ per count)			
	Channel 1	Channel 2	Channel 3	Channel 4
1	0.546789	0.219287	0.172192	0.192768
2	0.546550	0.219646	0.172358	0.192848
3	0.545936	0.219851	0.171731	0.192614
4	0.546007	0.220022	0.171502	0.192652
5	0.545903	0.220427	0.171879	0.192195
6	0.545664	0.221015	0.172338	0.191840
7	0.547264	0.221677	0.172380	0.191436
8	0.548600	0.222200	0.172600	0.191400
9	0.550227	0.222946	0.173572	0.191722

Finally, we note that these gains apply to the instrument in mid-July of 2002. We expect these gains to be quite stable, however, and periodic observations of the on-board lamps support this assumption between launch and the time of this writing (late September 2002). Periodic lamp observations, as well as new vicarious calibration campaigns will be made in the future to look for and track changes in the system.

APPENDIX

MISR Calibration Team Report

Prepared by Wedad Abdou, 13 September 2002

Band-averaged TOA radiances at railroad Valley
June 10 and 11, 2002

The Aqua space craft flew over Railroad valley (38.50 N and 115.69 W) on June 10 and 11. The geometry on these two days are shown in Table 1.

Table 1: Aqua Geometry on June 10 and 11, 2002.

Date	Time (UC)	Sun Zenith	Sun Azimuth	S/C zenith	S/C azimuth
June 10	20:19	17.68	212.33	45.57	75.3
June 11	20:56	23.06	234.08	21.56	260.87

The field data obtained at Railroad valley on June 10 and 11 includes:

1- The Portable Apparatus for Rapid Acquisition of Bidirectional Observations of Land and Atmosphere, PARABOLA, to measure the surface bidirectional reflectance factor, BRF, and hemispherical directional reflectance factor, HDRF, on a hemispheric grid of 5 degree resolution. The PARABOLA is mounted on a rod about 2 meters high. As shown in Figure 1 the instrument has two sensor heads and eight spectrally-filtered radiometers and is mounted on a rod ~2 meters high. A rectangular platform, mounted to the rod below the sensor heads, is used to place a Spectralon Panel to be used as a reference surface. The Spectralon has a near lamburtian reflectance and is used to calculate the surface HDRF. This is done by taking the ratio of the radiances reflected from the surface to that reflected from the Spectralon panel. Figure 2 is a surface plot of the PARABOLA data at the time of the Aqua overpass. In this figure the sun is shown at an azimuth angle of 212^o and a zenith angle of ~16.6^o. The radiance reflected from the Spectralon is shown at the zenith angle range of 0 to ~20^o. The PARABOLA data in that range are replaced by the average of the data surrounding the Spectralon panel. The shadow of the instrument mounting rod should appears at ~180^o from the Sun, i.e., at azimuth angle of ~32^o. However, it usually appears shifted by $\pm 5^o$ depending on which head sensor

is used. The shadow is clearly shown in Figure 3 which illustrates the HDRF as a function of the PARABOLA azimuth angle, at a view zenith angle of 16.6^o (the dotted line). The “hot spot”, a bright spot exhibited by some surfaces, appears opposite the sun position, i.e., at 180^o from the Sun, and at a view angle equal to the sun zenith angle. Therefore, the hot spot lies in the center of the instrument shadow. Correction of the shadow is very important if the surface exhibits a bright hot spot. The correction is implemented using various techniques depending on the brightness of the hot spot. In this case the data at the shadow was replaced by values collected at the view zenith angle of 21.78^o (dashed line). The HDRF values are then smoothed as shown by the solid line. The shadow-corrected PARABOLA data are then interpolated at a discrete number of viewing angles (16 in azimuth and 12 in zenith), and are expressed as a function of the viewing azimuth relative to the Sun azimuth (this HDRF format is required by the radiative transfer code which is used to determine the top of atmosphere radiances). Figure 4(a,b) shows the surface HDRF near the Aqua geometry on June 10 and 11. The maximum at 180 degree indicates the hot spot. Note that the surface HDRF values are almost the same for both days. However, Aqua azimuth angle with respect to the sun are 43^o and 207^o on June 10 and 11, respectively.

2- The portable spectrometer manufactured by Analytical Spectral Devices (ASD), to measure the surface HDRF in the nadir direction. Figure 5 shows the ASD data on June 10 and 11. The ASD data are used to normalize the PARABOLA data at the nadir.

3- The reagan sun photometer, to measure the atmospheric optical depth. The aerosol optical depth on the above dates are shown in Figure 6.

The above field data were used, with a validated radiative transfer (RT) code, to calculate the top of atmosphere (TOA) radiances. An aerosol model with a log-normal size distribution (mod radius = 0.07 micron and distribution width = 1.86) and a complex refractive index of 1.44 -0.005 i, was assumed in the calculations. The output of the RT code are the radiances relative to the solar irradiance, ρ, calculated at 27 wavelengths from 380 to 1028 nm, every 25 nm. The solar irradiance data, E_0, shown in Figure 7, are those published in the World Climate Research Program (WCRP) publication series No. 7, WMO ITD-No. 149, pp 119-126, October 1986.

The TOA band-averaged radiances are calculated using the equation:

$$TOAR = \frac{\int \rho E_0 R\lambda}{\int R\lambda}$$

where R is the Aqua response function at the wavelength λ. The Sun-Earth distance used in the calculations is 1.0154. The band-averaged TOAR for June 10 and 11 are listed in Table 2 and illustrated in Figure 8. The uncertainty in these results is ~ ±5%.

Table 2: Band-averaged TOA radiances (W/m2/micron/sr)

date	band 1	band 2	band 3	band 4
June 10	129.26	155.77	116.68	129.20
June 11	144.62	181.91	133.83	149.11

Figure 1.

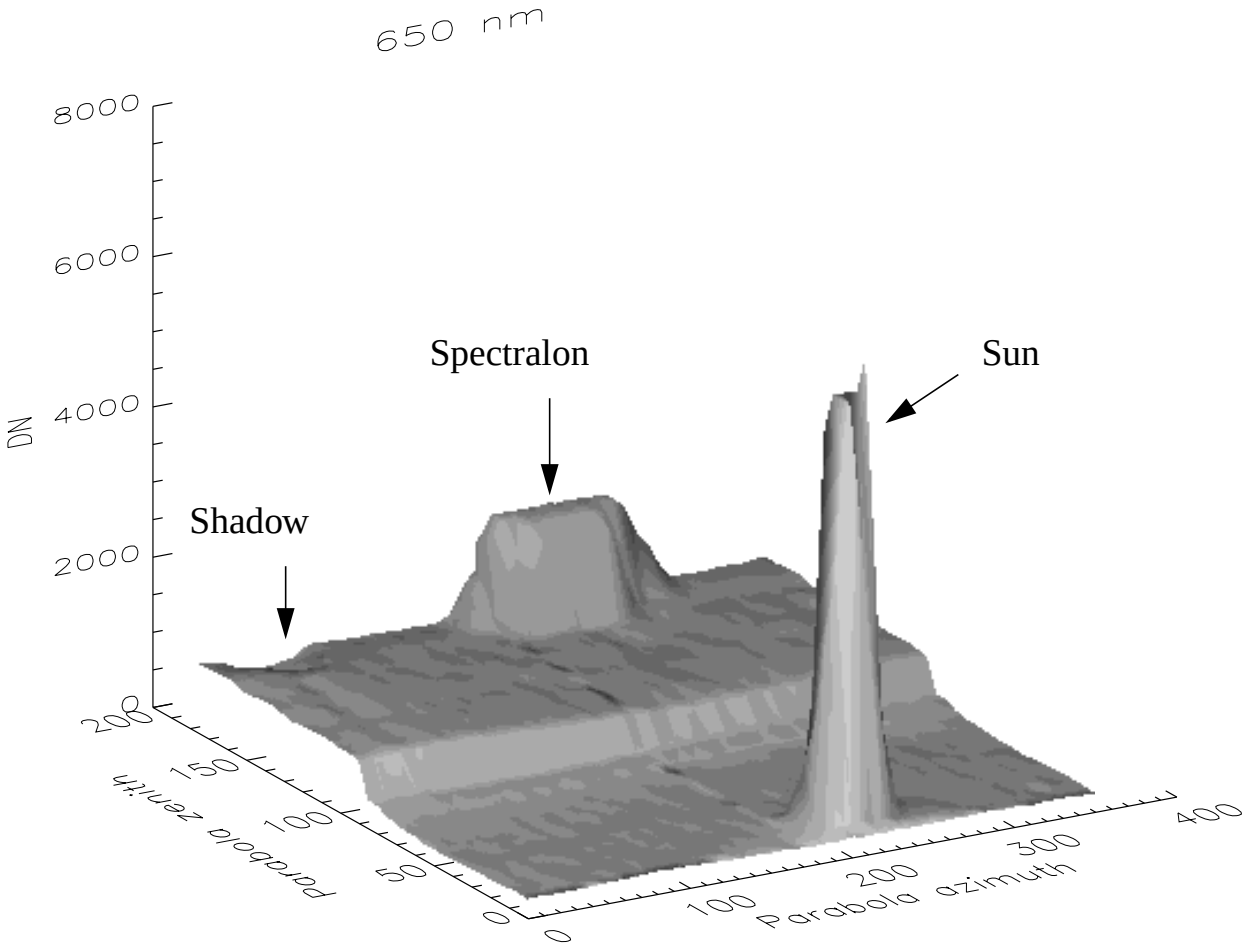
650 nm
8000
6000
4000
2000
DN
Spectralon
Sun
Shadow
200
150
100
50
0
Parabola zenith
0
100
200
300
400
Parabola azimuth

Figure 2.

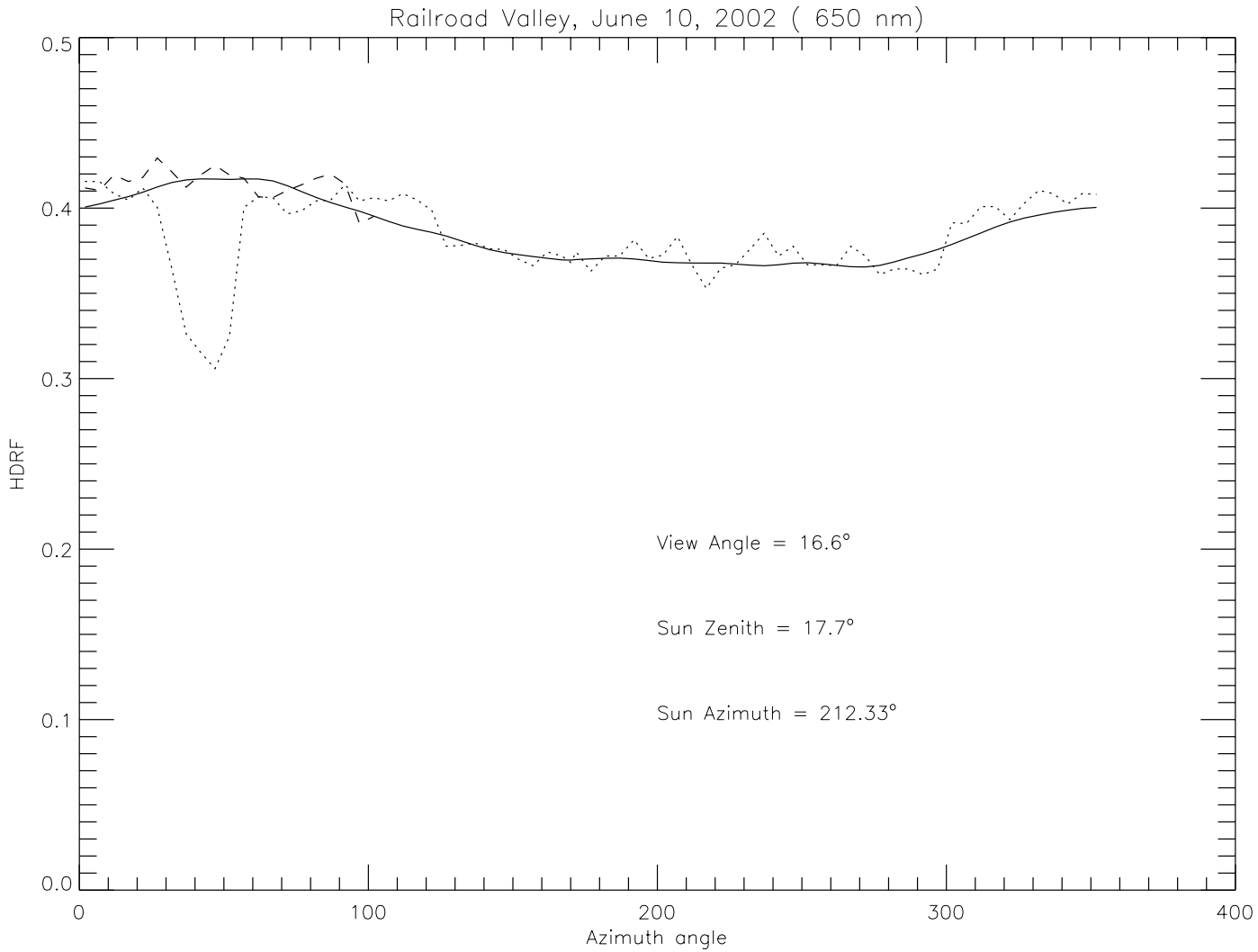
Railroad Valley, June 10, 2002 (650 nm)
HDRF
Azimuth angle
0.0
0.1
0.2
0.3
0.4
0.5
0
100
200
300
400
View Angle = 16.6°
Sun Zenith = 17.7°
Sun Azimuth = 212.33°

Figure3.

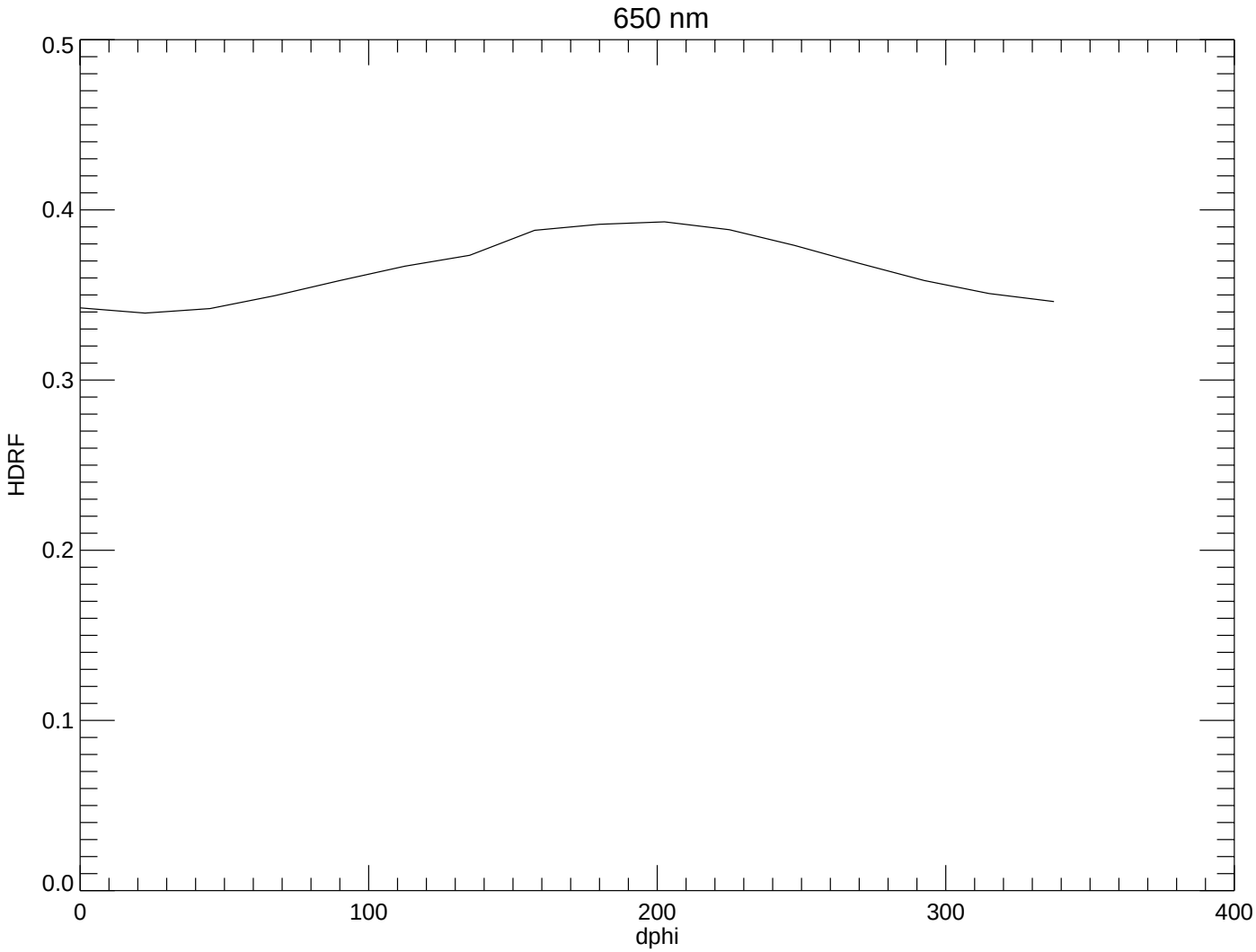

Figure 4a.

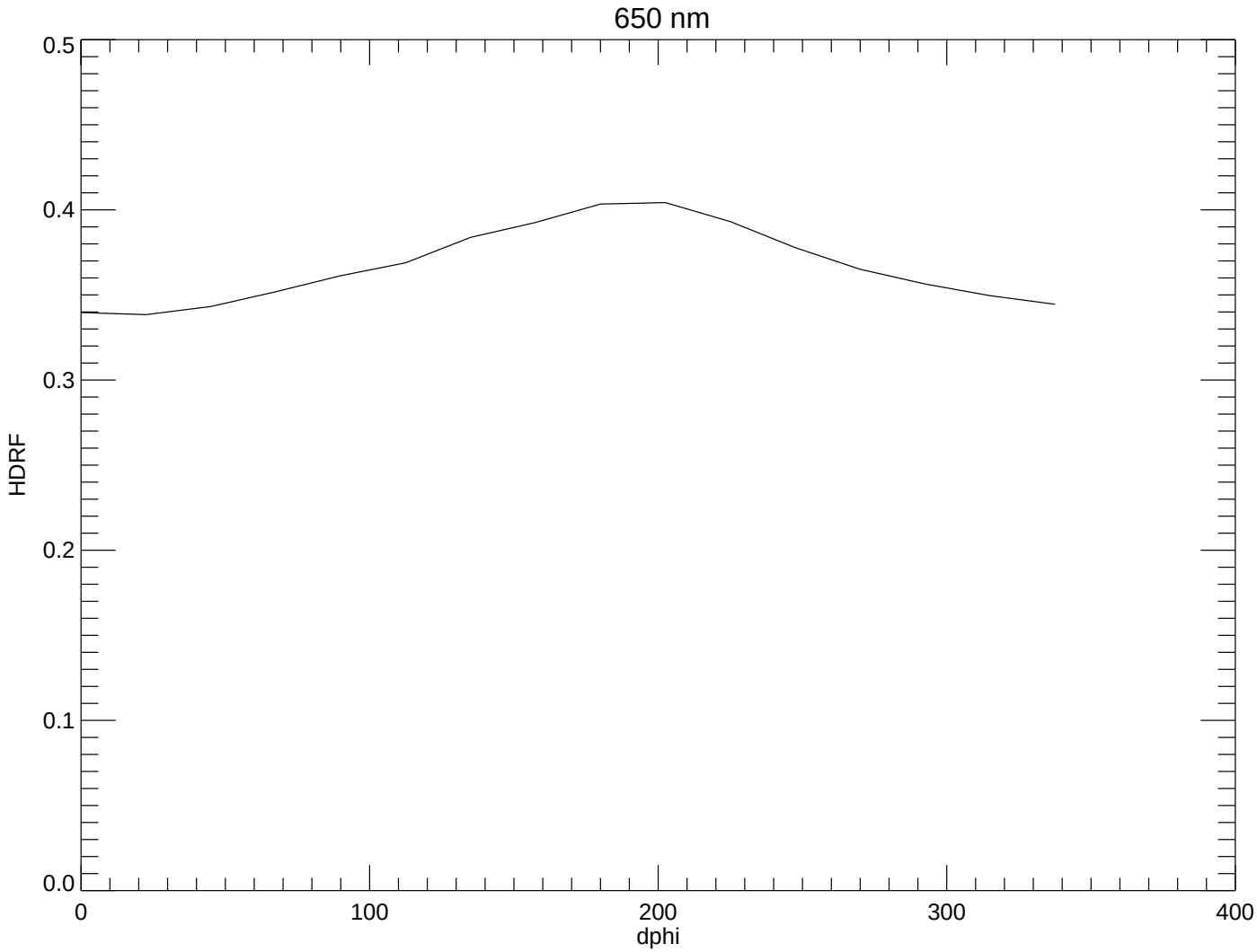

Figure 4b.

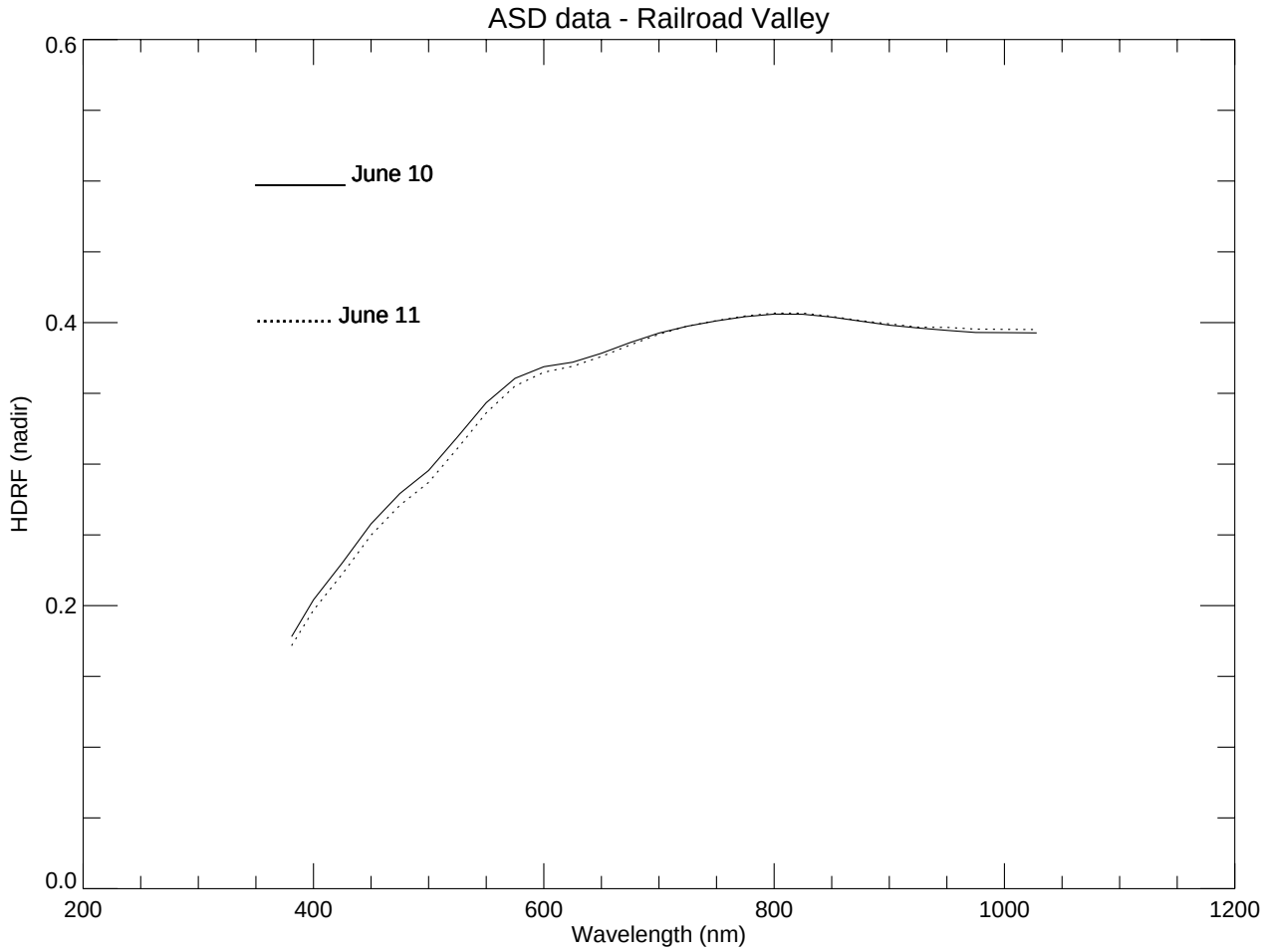
ASD data - Railroad Valley
June 10
June 11
HDRF (nadir)
Wavelength (nm)
0.0
0.2
0.4
0.6
200
400
600
800
1000
1200

Figure 5.

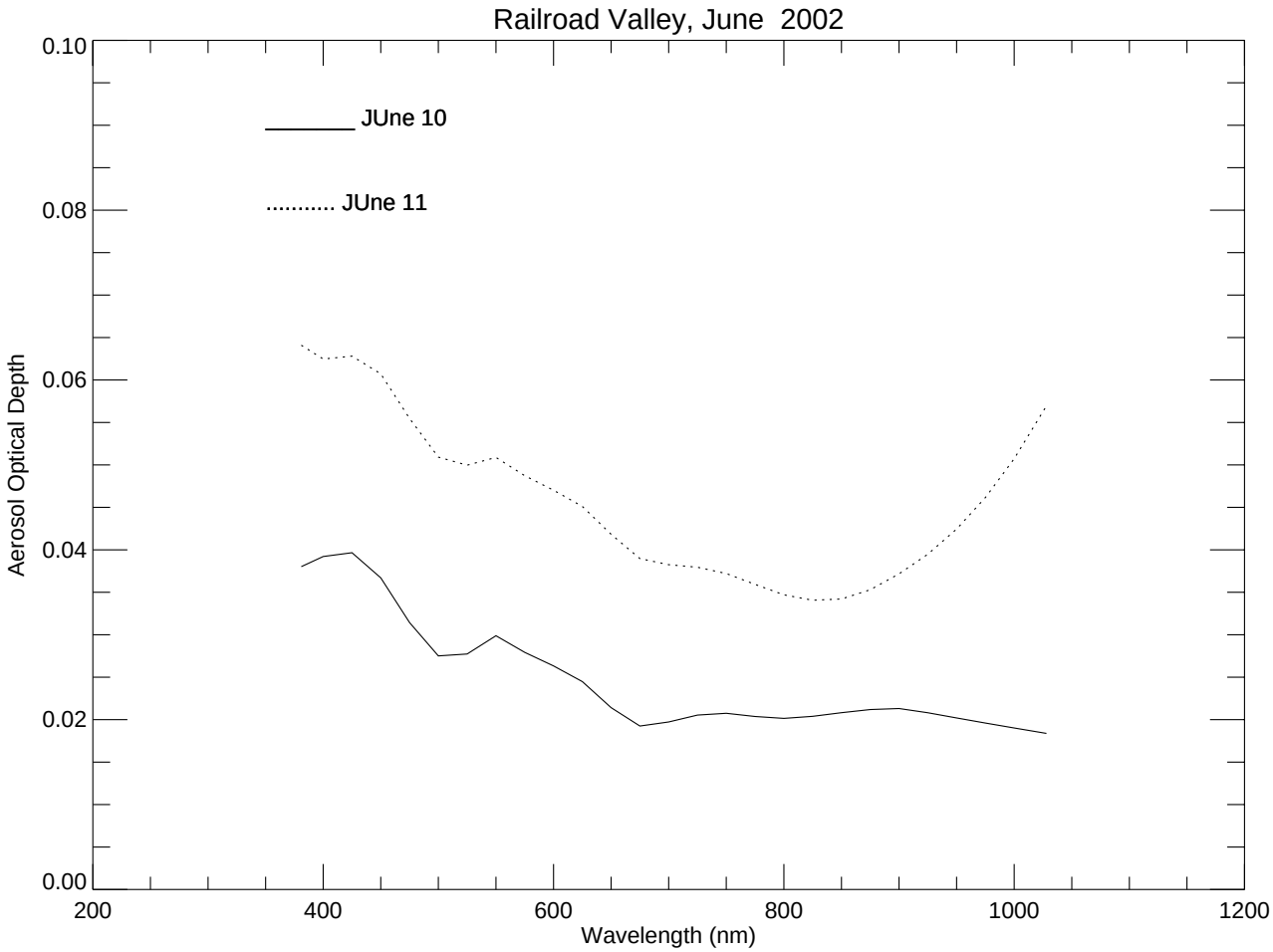
Railroad Valley, June 2002
JUne 10
JUne 11
Aerosol Optical Depth
0.10
0.08
0.06
0.04
0.02
0.00
200
400
600
800
1000
1200
Wavelength (nm)

Figure 6.

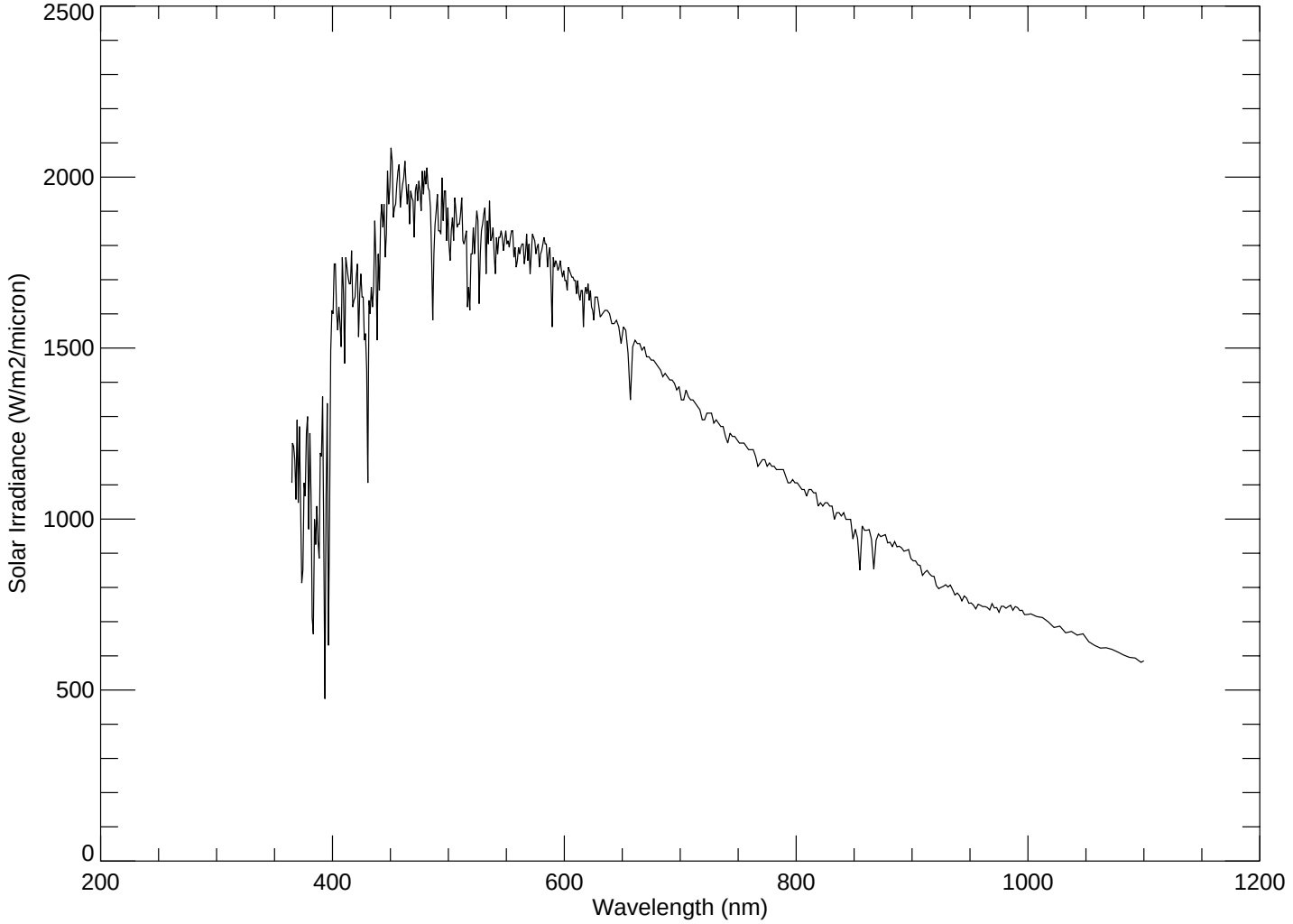
2500
2000
1500
1000
500
0
Solar Irradiance (W/m2/micron)
200
400
600
800
1000
1200
Wavelength (nm)

Figure 7.

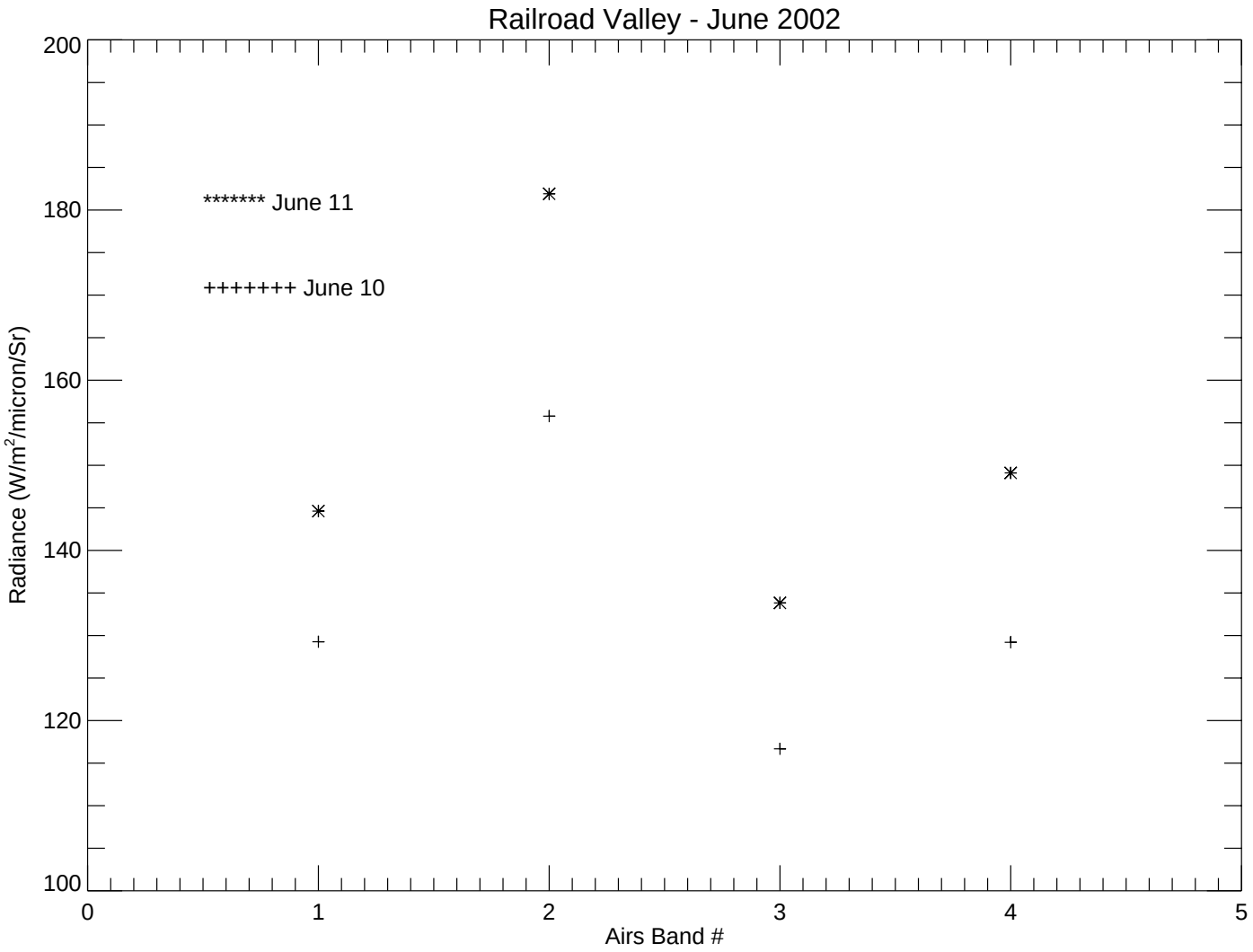
Railroad Valley - June 2002
******* June 11
+++++++ June 10
Radiance (W/m2/micron/Sr)
Airs Band #
200
180
160
140
120
100
0
1
2
3
4
5

Figure 8.